# Frequency-wavenumber migration of ultrasonic data

Young-Fo Chang [1] and Chir-Cherng Chern [2]

[1]Institute of Applied Geophysics, Institute of Seismology, National Chung Cheng University, Ming-Hsiung, Chia-Yi, Taiwan.

[2] Geophysical Data Processing Center, Offshore and Overseas Petroleum Exploration Division, Chinese Petroleum Corporation, Taipei, Taiwan.

**Journal of Nondestructive Evaluation, V19, N1, 1-10, 20000.**

Corresponding author: Young-Fo Chang
Tel: 886-5-272-0411 Ext. 6398
Fax: 886-5-272-0807
E-mail: seichyo@eq.ccu.edu.tw

# Frequency-wavenumber migration of ultrasonic data

Young-Fo Chang [1] and Chir-Cherng Chern [2]

[1] Institute of Applied Geophysics, Institute of Seismology, National Chung Cheng University, Ming-Hsiung, Chia-Yi, Taiwan.

[2] Geophysical Data Processing Center, Offshore and Overseas Petroleum Exploration Division, Chinese Petroleum Corporation, Taipei, Taiwan.

## Abstract

In ultrasonic nondestructive evaluation (NDE), the depth of the image is usually calculated by multiplying the traveling time of the echoes with the velocity of the medium. If the flaw is not a horizontal plane, the flaw images may be distorted and mislocated. Although the lateral resolution and sizing accuracy of the flaw image can be improved using the digital signal processing methods, e.g. the utilization of the blocking filter or deconvolution filter, these methods do a little favor about the distortion and mislocation problems.

The migration, an image processing method used widely in reflection seismology, is introduced to process the ultrasonic data in this study. Since the signals are coherent and the noises are random, the flaw image can be transformed from its apparent position to the true position using the migration method, and the resolution of the image may be improved.

Not only the real positions of the oblique cracks can be found upon applying the frequency-wavenumber (F-K) migration to process ultrasonic data, but also the dimensions of the flaws can be estimated more accurately. Results presented in this study show that the migration method can be applied successfully to the ultrasonic

data processing and can improve the quality of ultrasonic image in both size and location of the flaws.

Keywords: **Ultrasonic NDE, reflection seismology, migration.**

## Introduction

Because of the efficiency and economy, ultrasonic nondestructive evaluation (NDE) is a common method used to detect the flaws in materials[1,2]. The capability and resolution of ultrasonic NDE depend on both the applying hardware and the applying software. The main factors affected the resolution raising from the hardware are the transducer size, the beam width and the frequency bandwidth[3]. On the other hand, the software could be used to increase signal/noise (S/N) ratio of the ultrasonic data, and to improve the resolution of the image.

The digital signal processing methods that used most widely are block filtering and deconvolution for improving the resolution of scan image. While a deconvolution filter can eliminate the noise and enhance the useful signals, block filtering extracts the useful signals from the frequency domain[4]. Vollmann[5] used the Wiener deconvolution filter to improve a B-scan image. The C-scan image can also be processed by two-dimensional Wiener filter[4]. The deconvolution method can reduce the transducer blurring effects and improve the resolution of ultrasonic C-scan images[6,7].

The depths of flaws are estimated by multiplying the traveling time of the echoes with the velocity of the object. If the flaw faces are not horizontal planes, the locations and shapes of the flaw images may differ from the actual flaws. The blocking filtering and deconvolution can not do many efforts in this respect.

In the recent decades, Geophysicists have developed a number of valuable digital signal processing methods for seismic exploration. One of such methods involves the migration technique that moves signals from their apparent positions to true locations. This is now a basic procedure in the processing of seismic exploration[8,9]. It is not

necessary for the migration method to calculate an inverse filter. Just redistributes the signals into an appropriated space. Therefore, such a method can be regarded as one kind of the transformation technique. Ultrasonic NDT and seismic exploration use similar elastic wave theories to detect flaws and faults. The only difference between the two methods is the dimension of the wave and the targets. Consequently, it is possible to process the ultrasonic data utilizing the migration method.

In this research, the migration method used widely in reflection seismology will be applied to process the ultrasonic data. Three different kinds of flaws with the different dip angles, depths, and sizes were studied in this experiment.

## Theory and data process

The single-probe pulse-echo method is usually used in ultrasonic NDE. If the crack is oblique, the crack image will be distorted and mislocated by multiplying the traveling time of the echoes with the velocity of the medium. Figure 1 exhibits the geometric relationship between an oblique crack (shown as line ab) and the crack image (dashed line a′b′). When the probe is scanning at $P_1$, the point on the crack reflecting the echo will be located at point a. However, the apparent location of the reflection point will be point a′ in the scan image because the ray path A is equal to A′. That is the same when scanning at $P_2$, the true reflection point b on the crack will be mislocated to point b′ displayed in the scan image. Therefore, the scanned section shows the apparent position a′b′ for the flaw. The apparent length a′b′ of the crack is longer than the true one, i.e. ab, and the apparent dip angle θ′ is less than the true dip angle θ. In the case of a point flaw within the material, the scanning shape for the point flaw would be like an “umbrella”. Such a case has been shown in Figure 2. When the transducer is scanning at P, the scattered echo from the point flaw “a” will

be displayed at the point “a′”, where is below P directly and ray path A = A′, in the scan image. If the probe continue to advance, the “umbrella”, the dashed line bb′ as shown in Fig. 2, will develop. Consequently, once we transformed the traveling time to the depth for imaging by multiplying the traveling time of the echoes and the velocity of the material together, the flaw images can not correlate to their true configurations.

The migration of seismic data, that transforms the seismic events from their apparent positions to the true locations, is a basic and important data processing procedure used in exploration seismology. There are a lot of migration methods based on different theories and approximations, and each migration method has its advantages to deal properly with the associated cases. If the earth has no (or little) lateral velocity change, the appropriate frequency-wavenumber (F-K) migration is a fast and powerful migration method [10,11]. It is the case of our specimens tested in this study that have no lateral velocity change, and the F-K migration method is satisfactory for migrating the ultrasonic data.

The development history and the theory of the migration techniques could be found in the literature[8,9,10]. Only the major transformations of the F-K migration are outlined here. If the B-scan was carried out along the x-axis on the specimen surface, the echoes in some time gates that we are interesting can be stored in hard disk. Since the velocity of the duralumin is known, the traveling time of the echo can be transformed into the depth by $z = 2tV$, where z, t and V are respectively the depth, the traveling time of the echo, and the velocity of the duralumin. After constructing the B-scan section, $u(x,z)$, the section in wavenumber domain, $F(k_x,k_z)$, can be obtained using the following 2-D Fourier transform:

$$F(k_x, k_z) = \iint u(x,z) e^{-i(xk_x + zk_z)} dxdz.$$

where $k_x$ and $k_z$ are the wavenumbers for the x- and z- axes. A mathematical expression of the migration process ( $(k_x, k_z) \rightarrow (\bar{k}_x, \bar{k}_z)$ ) could be written as[11] :

$$\bar{F}(\bar{k}_x, \bar{k}_z) = \frac{k_z}{\sqrt{k_x^2 + k_z^2}} F(k_x, \sqrt{k_x^2 + k_z^2})$$

where $\bar{F}$, $\bar{k}_x$ and $\bar{k}_z$ are respectively the migrated section in the wavenumber domain, and the two migrated wavenumbers for the x- and z-axes. After migration, the point where the line-cracks intercepted the x-axis is the same. The mapping leaves the spatial frequency invariant. Thus, one must have $k_x = \bar{k}_x$. On the other hand, the change from the apparent dip angle to the true dip angle is the mapping $\bar{k}_x / \bar{k}_z = k_x / \sqrt{k_x^2 + k_z^2}$. Since $k_x = \bar{k}_x$, the $\bar{k}_z$ can be calculated by $\bar{k}_z = \sqrt{k_x^2 + k_z^2}$. Before the migration, the event occupies more area. Therefore, the event must be multiplied by the weighting factor to restore the correct balance after migration, and $k_z / \sqrt{k_x^2 + k_z^2}$ is the weighting factor.

The migrated section in wavenumber domain, $\bar{F}$, can be transformed into the migrated space domain ( $\bar{u}(\bar{x}, \bar{z})$ ) by inverse Fourier transformation

$$\bar{u}(\bar{x}, \bar{z}) = \iint \bar{F}(\bar{k}_x, \bar{k}_z) e^{i(\bar{x}\bar{k}_x + \bar{z}\bar{k}_z)} d\bar{k}_x d\bar{k}_z$$

where $\bar{x}$ and $\bar{z}$ are the migrated x- and z-axes. Then, the migrated B-scan can be constructed and the images of the flaws within it may correlate considerably to their real configurations.

In this research, the F-K migration of the ultrasonic data was done at the Geophysical Data Processing Center, Offshore and Overseas Petroleum Exploration Division, Chinese Petroleum Corporation.

## Apparatus

The testing apparatuses are essentially similar to that used elsewhere in nondestructive evaluations and their schematics are shown in Figure 3. The 20 MHz contacted longitudinal wave transducer (Panametrics V116) with a diameter of 0.125 inch was used in the experiments and it was excited by a pulser/receiver (Panametrics 5058PR) operating in the pulse-echo mode. The digital oscilloscope (Tektronix 11402A) surveyed and recorded the signals, and a personal computer read the digital signals from the oscilloscope. The survey lines were on the top surface of the specimens using honey as the couplant to improve the coupling conditions. The measurements were artificial and the sampling rate in space was 1 mm.

## Specimens and experimental results

Four specimens were examined in order to simulate the different flaws in the objects. Duralumin was used as the master material and its longitudinal wave velocity is 6623 m/sec.

### 1. Oblique cracks

The transducer used in this experiment is not infinitely small and its beam width is not a line. When the dip angle of the oblique crack is not large, the echoes reflected from the oblique crack can be still detected by the transducer. However, the crack image will locate on the incorrect position.

The first two specimens are oblique cracks, the dip angles are 15° and 30° shown in Figures 4a and 5a, respectively. The corresponding B-scans are shown in Figures 4b and 5b. The migrated sections for the dip angles of 15° and 30° are shown in Figures 4c and 5c, respectively. The dashed lines in Fig. 4 and Fig. 5 are the true positions of the cracks. In these figures the apparent dip angle is less than the true dip

angle, and as the dip angle becomes steeper the difference between the angles increases. The energy of the echoes that reflected from the crack with a dip angle of 30° is smaller than that reflected from the one of 15°. Therefore, the image of the apparent crack in Fig. 4b is clearer than that in Fig. 5b. Even the multiple reflections (MR) reflected between the top surface and crack can be seen in the Fig. 4b on the left-top corner. It should be noted that the migrated sections, as shown in Figures 4c and 5c, reveal that the crack images have migrated to their true positions.

Although the migration technique can not eliminate the energies of multiple reflections, the signals of multiple reflections in Fig. 4c are obscurer than those ones shown in Fig. 4b. This is because of that the apparent velocity of the multiple reflections is not the same as the velocity of the primary reflections. In Fig. 5b the repeated horizontal events across the section are the side lobes of the source waveform. The amplitudes of the side lobes are the same order as the echoes reflected from the crack. In this case, the S/N ratio is small and the quality of the migrated flaw image is reduced. The migrated crack image in Fig. 5c is thus obscurer than that one in Fig. 5b. However, the position of the crack is accurately estimated in the migrated section.

## 2. Different depth flaws

If the sound beam spread out, the images of the point flaws at different depths are different in both size and clarity. The image of the shallow point flaw is smaller and clearer than the deep one even though the flaws are the same size. Therefore, it is not easy to read the sizes of the flaws directly from B-scan. In this section, the B-scan of five through-holes with diameters of 2 mm at the different depths of 5, 10, 15, 20 and 25 mm are studied. The specimen and B-scan are shown in Fig. 6a and b, respectively. The image of the shallowest hole is in the dead zone and so it is not

shown in the B-scan. The image located at x = 30 mm and depth = 20 mm is the first multiple reflection of the echoes between the surface of the specimen, and the hole located at x = 30 mm and depth = 10 mm. In Fig. 6b, the case of the deeper holes, the curvature, size and clarity of the flaw images become smoother, larger and lower. The migrated section is shown in Fig. 6c, and all flaw images have been recovered to the true size, i.e. 2 mm.

The migrated images (Fig. 6c) of the multiple reflection of the holes appeared at position x = 10 mm, depth = 10 mm and x = 30 mm, depth = 10 mm are clearer than that in Fig. 6b. This is because of that the curvature of the “umbrella” of multiple reflections still satisfies the travel time curve for the diffraction pattern of a point scatter. Consequently, the flaw images of the multiple reflections can be focused by the migration method.

## 3. Different size flaws

If the size of the flaw is not largely greater than both the wavelength of the echo and the size of the transducer, the flaw image in the B-scan will be like an “umbrella” which are the diffracted echoes from the flaw. The size of the flaw is not always correlated to the size of the "umbrella". Therefore, it is difficult to find directly the actual size of the flaw from the B-scan. A specimen, as shown in Fig. 7a, with 5 through-holes (the diameters are 1, 2, 3, 4 and 5 mm respectively) was scanned. The depths of the center of the holes are all at 20 mm. The B-scan is shown in Fig. 7b. The sizes and curvatures of the 5 “umbrellas” are almost the same, even though the diameters of the through-holes are different. It is not easy to evaluate the sizes of these holes from these images. This means that the echoes detected by the transducer are dominantly the diffracted waves that diffracted from the top of the holes. After migration shown in Fig. 7c, the shapes of the holes could not be still constructed and

the images of the holes are the same size. This is because the echoes reflected or diffracted from the other areas of the holes never come back to the probe except those ones from the top area of the holes.

The contrast between the amplitudes of the echoes diffracted from the different flaws is small. Also, the ultrasonic data were grided, smoothed and colored for imaging, and reduced the differentiation. Therefore, the size of the flaws can not be differentiated by their images. In an ideal case, the echoes reflected from the bigger holes will have the larger amplitudes. The A-scan therefore may reveal the size of the hole. Figures 8a and 8b are respectively part of the original and migrated A-scans. The numbers on the top of the A-scans are the relative sizes of the amplitudes of the echoes detected directly above the holes. The relationship between the peak amplitude of the echoes and the diameter of the holes is shown in Fig. 9. The amplitude of the echo reflected from the hole with a diameter of 2 mm seems large, while the one, reflected from the 3 mm-diameter hole, is too small in the original A-scans. This unpredictable and bursted error of the amplitude during the artificial scan can be usually found due to the change of the coupling condition and the uncertainty of the probe position. It can be thought of the migrated A-scan as the result that takes the summation of the echoes distributed on the diffracted curvature. After migration, the unpredictable and bursted errors can be reduced in the migrated A-scans. The migrated amplitudes thus shown in Fig. 9 (solid circle) are more reasonable than the original data, and the result can be used to estimate the size of the holes more accurately.

## Discussion

If the sound beam emitted by the transducer is the line-like one, only the

horizontal crack below the transducer can be detected and there is no migration problem. The sound beam emitted by common transducer used is indeed narrow in the near field distance, but spreads out in the far field distance. Therefore, the flaw, not a horizontal crack, can be detected. When the sound beam is a narrow one, only a small area below the surface can be scanned and only the limited information can be obtained. When the sound beam is broad, large area can be scanned and a lot of information below the surface can be received. However, the information may be very weak and complex, and it is not easy to utilize. Owing to the progress of the electronics industry and the digital signal process, recently it becomes possible to process/migrate the weak and complex information received by broad sound beam transducer. After processing/migrating, the resolution of the information can be enhanced.

The equation of the migration is derived for a point source radiating spherical waves. Theoretically, the energy of the waves within the spherical wavefront, instead of within the sound beam, is incoherent. It can not be focused in the migrated section after transformation. Therefore, although the transducer used in the experiments is not point source, this method can work. In order to reduce the effect of over-migration in the processing, we usually restrict within some distance in accordance with the sound beam that the echoes can be migrated/transformed.

Since the sound beam used in this study is not infinitely narrow, not only where the center of the transducer located directly above the flaw can record the echo reflected from the flaw, but also the echoes reflected from the horizontal crack can be detected. Hence, the migration can work. If the flaw is shallow or is located in the near field distance, the migration techniques can do only minor improvement for the resolution of the image since only small information about the flaw was obtained in

the scanning. Fortunately, the distortion and mislocation problems for the flaw images are also minor in such situation. If the flaw is deep or in the far field distance, the distortion and mislocation of the flaw image is great. In such a case, large useful information about the flaw can be gotten in the scanning. Then, migration can do great improvement for the resolution of the image.

It is not easy to completely construct the images of the flaws in both shape and location from finite shooting- and receiving-positions and viewing-angles. The echoes reflected or diffracted from the bottom and side of the holes never come back to the probe. Hence, the configurations of the holes can not be reconstructed in the migrated section as shown in Fig. 6c and Fig. 7c. Cracks with the dip angles of 45° and 60° had been also scanned. Since the crack images could not be seen in these sections, the sections are not shown in this paper. This is because the echoes reflected from the cracks are too weak to detect. In order to pick up the reflected echoes from a steep oblique crack, a double-probe with an offset between the probes must be used.

The performance of the migration depends on the theory used, geometry of the flaw, data coverage of the detecting area, S/N ratio, velocity distribution in the object, sampling rate in both the space and time domain and the fluctuations of the waveforms. All these factors affect the clearness of the migrated images, and so the flaw images in the migrated sections may be a little blurred than those in the original sections as shown in Fig. 4c and Fig. 5c. However, the shapes, sizes and locations of the flaws shown in the migrated sections are the more realistic representations of their true conditions than those ones in the original sections.

Real situations may be more complex than this paper discussed. Diverse flaws may exist in an object in the meantime. While the echoes reflected or diffracted from the flaws may mix with each other, migration can still work properly. The more

diverse the flaw, the more ultrasonic data are required for the migration process in order to make a correct estimation. The geometry of the flaws is three dimensions and so the effects affecting the flaw images are also three-dimensional. If the time histories of the C-scan had been stored in a storage medium, a 3-D migration method, which is used in 3-D reflection seismology (8,9,10), can also be applied to the C-scan data.

## Conclusion

In the ultrasonic NDE, we usually calculate the depth of a section according to multiply the traveling time of the echoes by the velocity of the object. The images of the flaws, however, will be distorted when they are not horizontal plane flaws. From the results of this research, the images of oblique cracks can be located to their true positions and the sizes of the flaws can be estimated more accurately by applying the migration technique. The shapes, sizes and positions of the flaws exhibited in the migrated section are more realistic than those ones in the original section. In this study, we have proved that the migration technique can be successfully applied to ultrasonic data. It provides a powerful and useful method to improve the accuracy of estimating the flaws in ultrasonic NDE.

## Acknowledgment

This work was supported by the National Science Council of the Republic of China under Grant NSC 86-2116-M-194-007T.

## References

1 **Bray, D. E. and Stanley, R. K.**, *Nondestructive evaluation*, McGraw-Hill, New York, 1989.

2 **Blitz, J. and Simpson, G.**, *Ultrasonic methods of non-destructive testing*, Chapman & Hall, London, 1996.

3 **Silk, M. G.**, *Ultrasonic transducers for nondestructive testing*, Adam Hilger, Bristol, 1984.

4 **Zhao, J., Gaydecki, P. A. and Burdekin, F. M.**, 'Investigation of block filtering and deconvolution for the improvement of lateral resolution and flaw sizing accuracy in ultrasonic testing', ***Ultrasonics***, 33 (1995) pp. 187-194.

5 **Vollmann, W.**, 'Resolution enhancement of ultrasonic B-scan images by deconvolution', ***IEEE Trans Sonics Ultras*** **SU29**, 3 (1983) pp. 78-83.

6 **Cheng, S. W. and Chao, M. K.**, 'Resolution improvement of ultrasonic C-scan images by deconvolution of the cross-beam pattern of transducer', ***Proc. 8th Asia-Pacific Conference on Nondestructive Testing (8th APCNDT)***, Taipei, December 11-14 (1995) pp. 615-622.

7 **Cheng, S. W. and Chao, M. K.**, 'Resolution improvement of ultrasonic C-scan images by deconvolution using the monostatic point-reflector spreading function (MPSF) of the transducer', ***NDT & E International***, 29 (1996) pp. 293-300.

8 **Dobrin, M. B. and Savit, C. H.**, *Introduction to geophysical prospecting*, McGraw-Hill, 4th edn, New York, 1988.

9 **Yilmaz, O.**, *Seismic data processing*, Society of Exploration Geophysicists, Tulsa, 1987.

10 **Gardner, G. H. F.**, *Migration of seismic data*, Society of Exploration Geophysicists, Tulsa, 1985.

11 **Chun, J. H. and Jacewitz, C. A.**, 'Fundamentals of frequency domain migration', *Geophysics*, 46 (1981) pp. 717-733.

## Figure captions

Figure 1 An oblique crack shown as line ab exhibited in the B-scan will locate at the apparent position presented as dashed line a′b′.

Figure 2 The images of a point flaw “a” in the B-scan would appear as ‘umbrella’ which are displayed as dashed lines bb′.

Figure 3 The ultrasonic scanning system used in the experiments.

Figure 4 (a) A specimen with a 15° oblique crack; (b) the original B-scan; (c) the migrated B-scan.

Figure 5 (a) A specimen with a 30° oblique crack; (b) the original B-scan; (c) the migrated B-scan.

Figure 6 (a) A specimen with different depths but same size through-holes; (b) the original B-scan; (c) the migrated B-scan.

Figure 7 (a) A specimen with different size through-holes; (b) the original B-scan; (c) the migrated B-scan.

Figure 8 A part of the A-scans for specimen Fig. 7a. (a) original A-scans; (b) migrated A-scans.

Figure 9 The relationship between the diameter of the through-holes and the amplitude of the echoes detected above the holes.

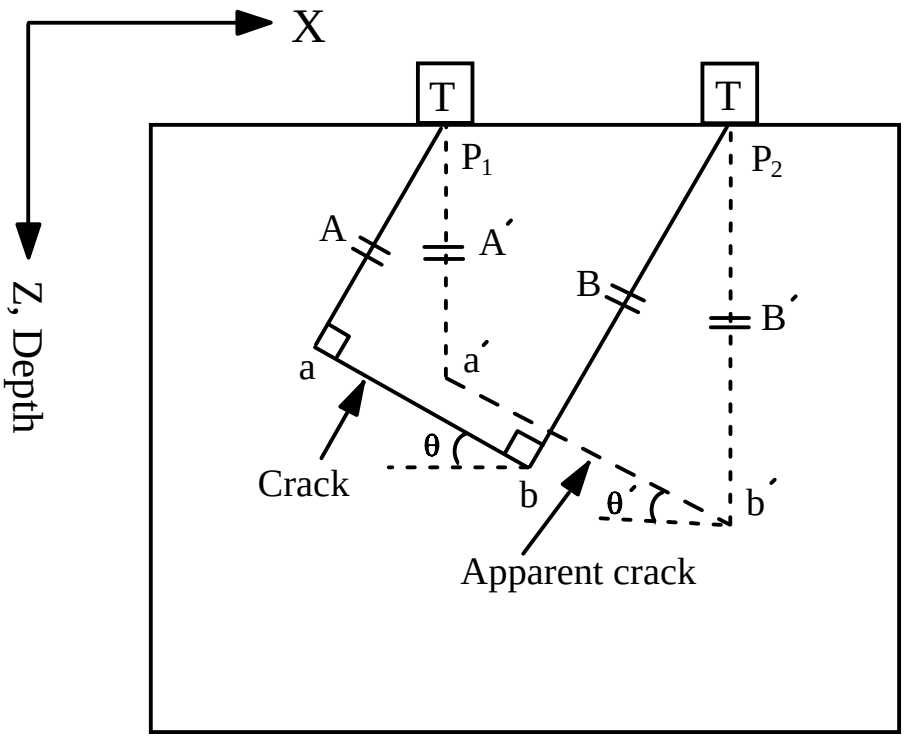
X
Z, Depth
T
T
P1
P2
A
A´
B
B´
a
a´
θ
Crack
b
θ´
b´
Apparent crack

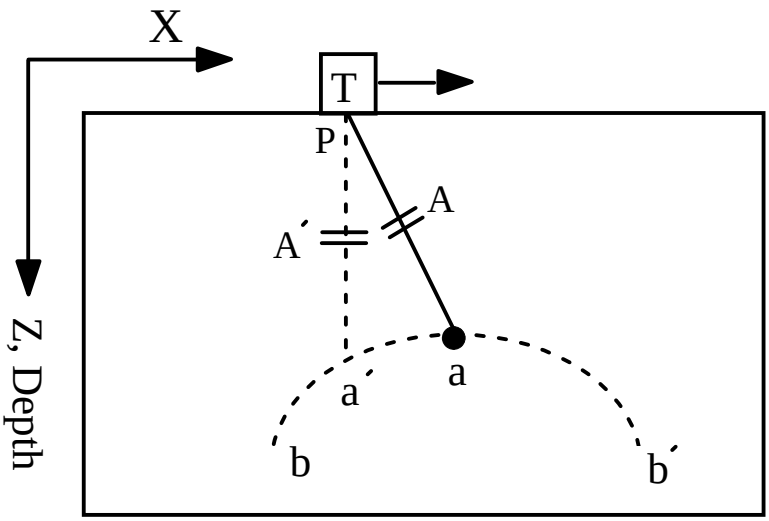
X
T
P
A
A´
Z, Depth
a
a´
b
b´

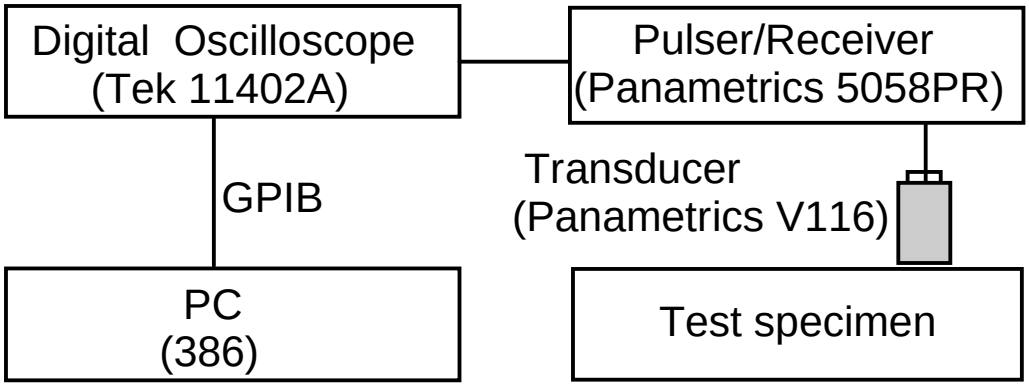
Digital Oscilloscope
(Tek 11402A)
Pulser/Receiver
(Panametrics 5058PR)
GPIB
Transducer
(Panametrics V116)
PC
(386)
Test specimen

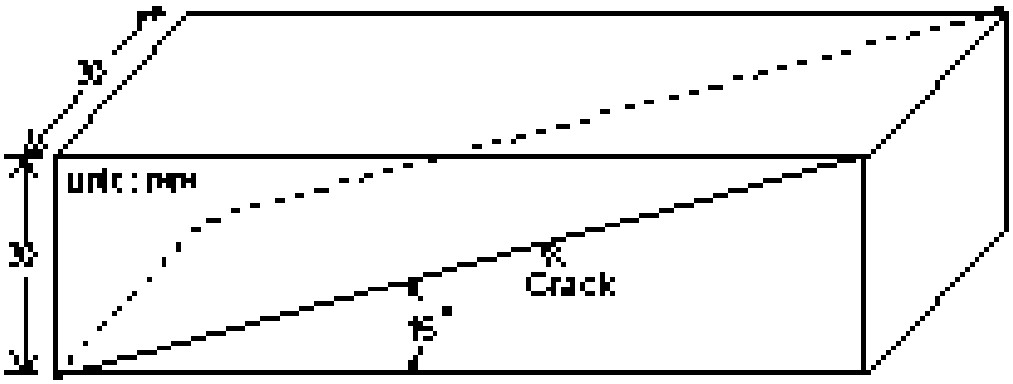
unit : mm
Crack

(a)

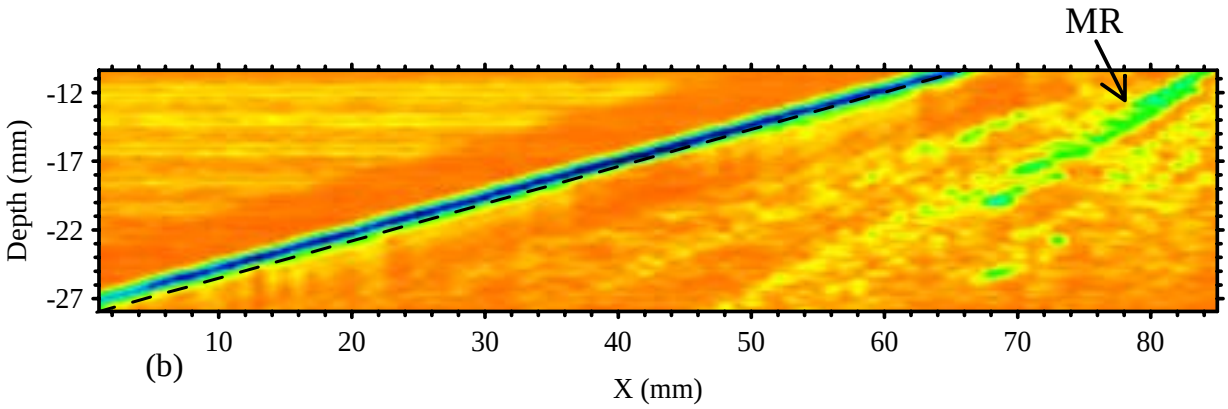
MR
Depth (mm)
-12
-17
-22
-27
10
20
30
40
50
60
70
80
X (mm)

(b)

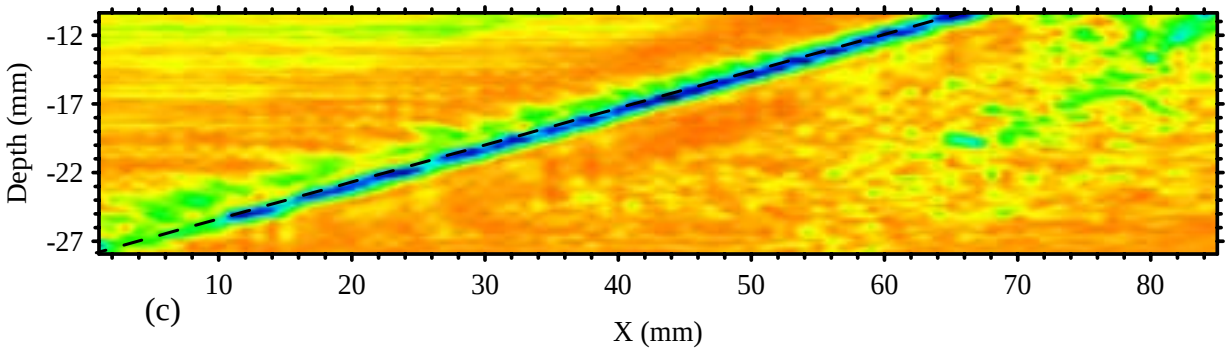
Depth (mm)
-12
-17
-22
-27
10
20
30
40
50
60
70
80
X (mm)

(c)

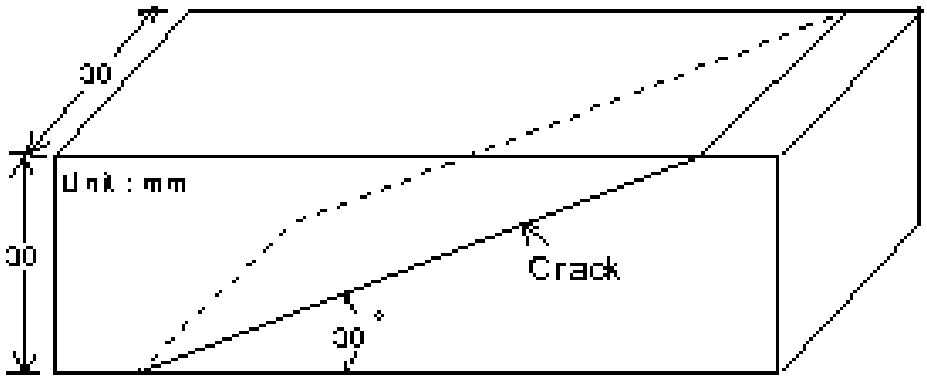
30
Unit : mm
30
Crack
30
°

(a)

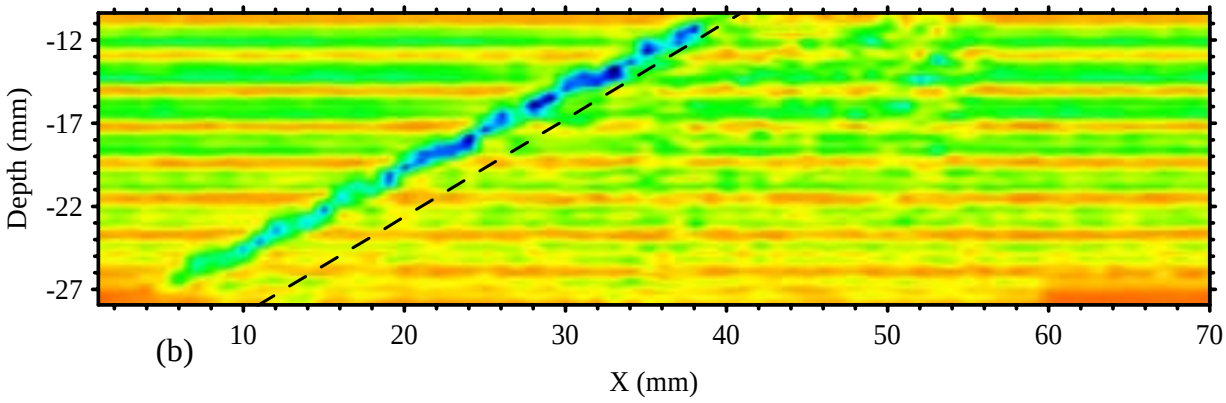
-12
-17
-22
-27
Depth (mm)
10
20
30
40
50
60
70
X (mm)

(b)

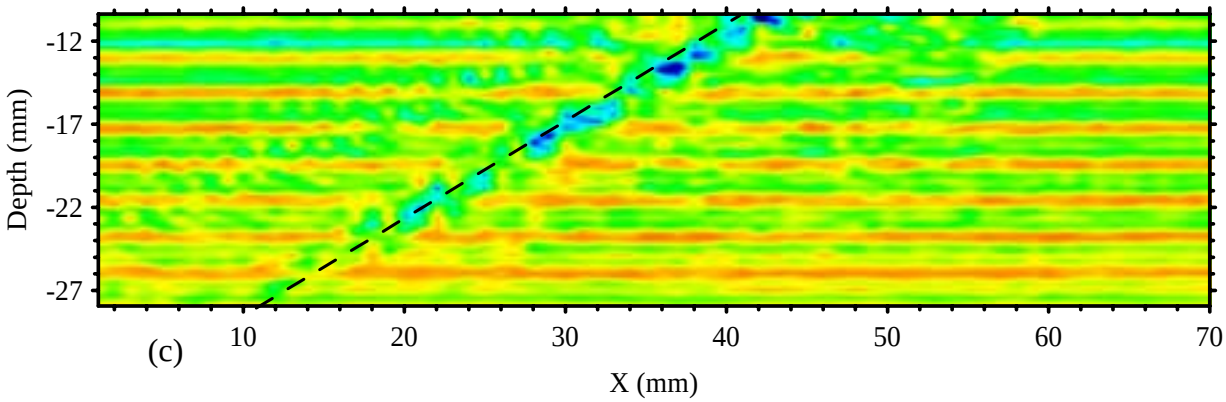
-12
-17
-22
-27
Depth (mm)
10
20
30
40
50
60
70
X (mm)

(c)

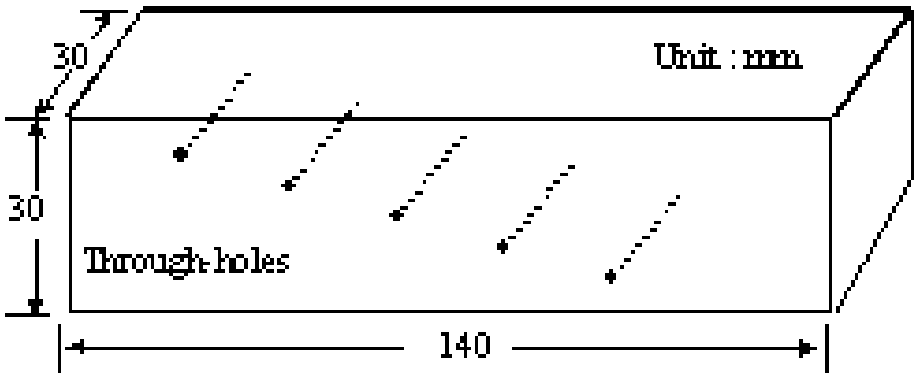
30
Unit : mm
30
Through-holes
140

(a)

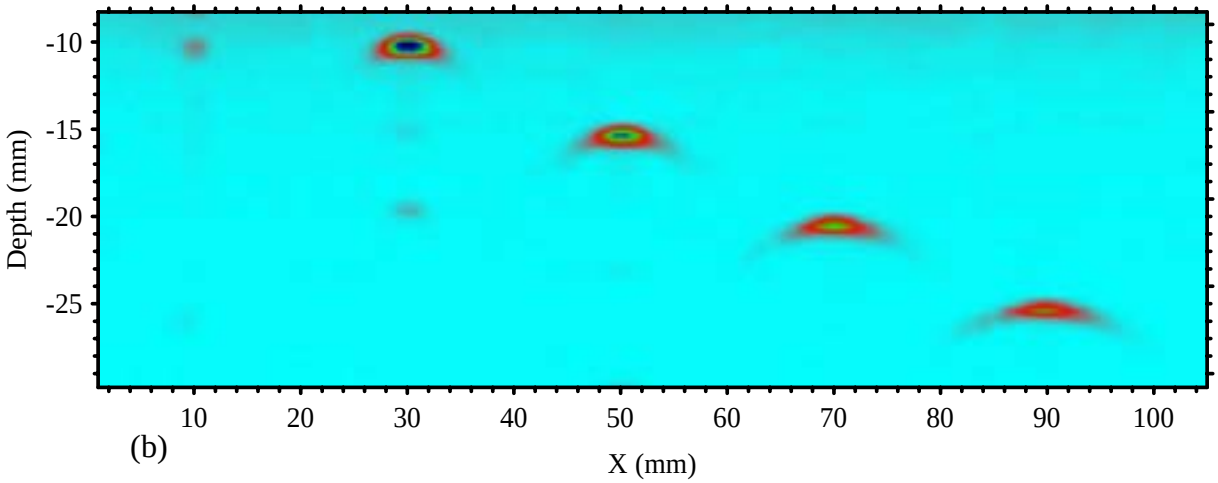
-10
-15
-20
-25
Depth (mm)
10
20
30
40
50
60
70
80
90
100
X (mm)

(b)

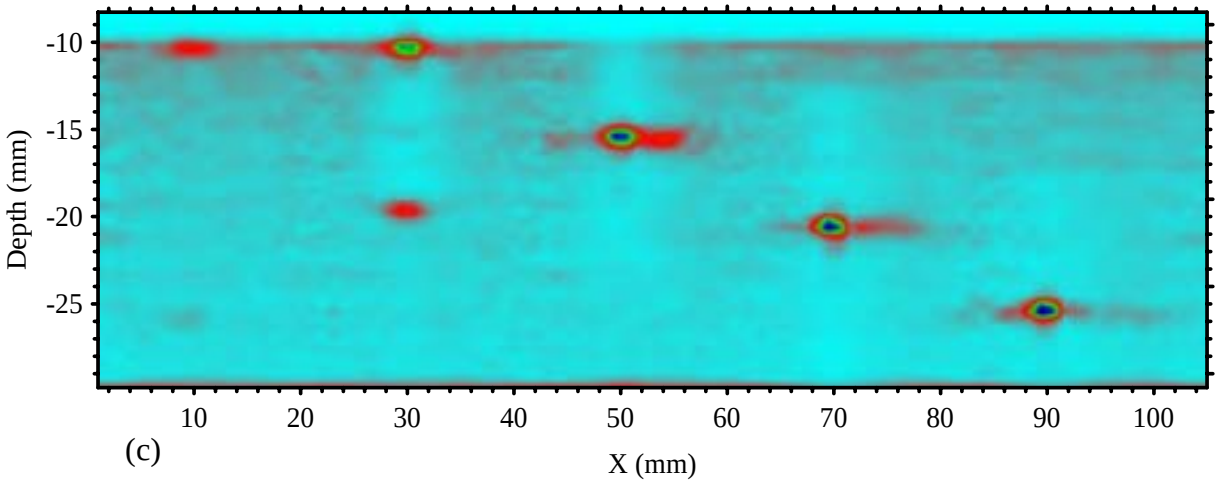
-10
-15
-20
-25
Depth (mm)
10
20
30
40
50
60
70
80
90
100
X (mm)

(c)

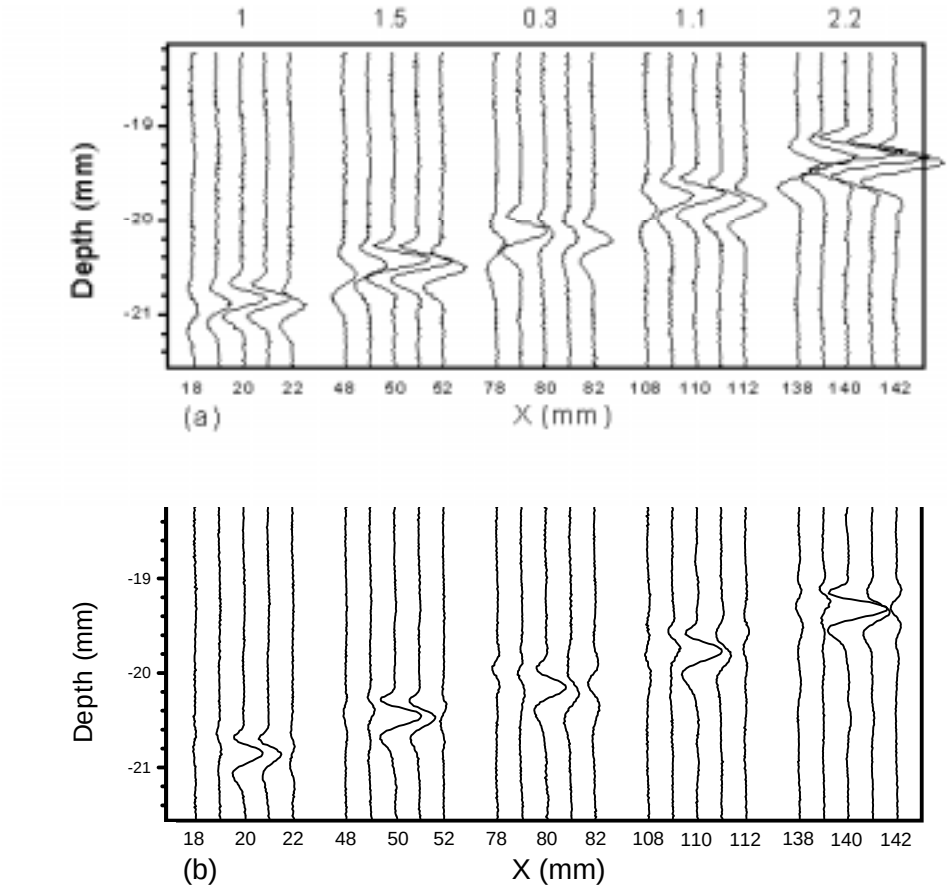
1
1.5
0.3
1.1
2.2
Depth (mm)
-19
-20
-21
18 20 22 48 50 52 78 80 82 108 110 112 138 140 142
(a)
X (mm)
Depth (mm)
-19
-20
-21
18 20 22 48 50 52 78 80 82 108 110 112 138 140 142
(b)
X (mm)

Fig. 8

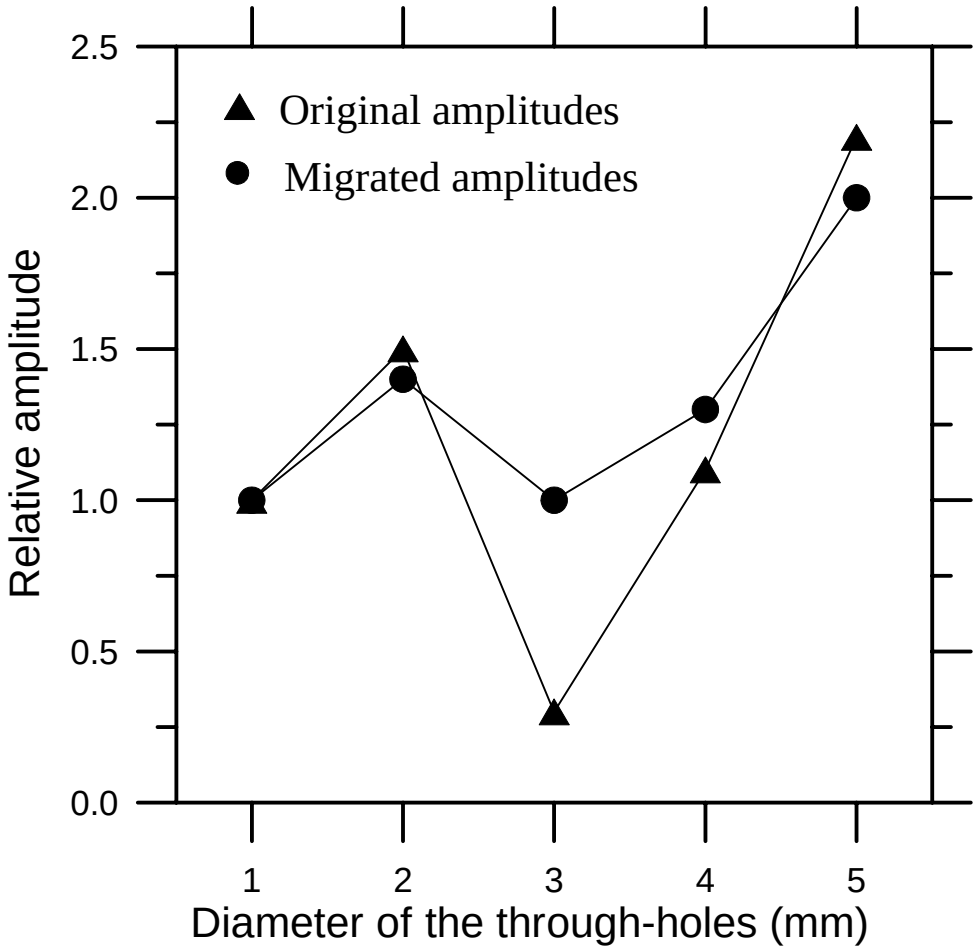
Original amplitudes
Migrated amplitudes
Relative amplitude
2.5
2.0
1.5
1.0
0.5
0.0
1
2
3
4
5
Diameter of the through-holes (mm)

Fig. 9